ACCURACY BUDGET AND PERFORMANCES

J.H.J. de Bruijne*

European Space Agency, Astrophysics Missions Division, ESA-ESTEC, 2200AG Noordwijk, The Netherlands

ABSTRACT

Gaia's scientific objective can be summarised as: to observe the complete sample of all stars brighter than $V \sim 20$ mag with end-of-life astrometric accuracies of 10 μas at $V = 15$ mag. To first order, Gaia's astrometric capabilities are a function of the satellite's operational strategy (mainly scanning law and mission lifetime) and the properties of its optical and detector system (e.g., CCD time-delayed integration). This paper elaborates on the following points:

1. As a result of the scanning law, astrometric accuracies vary with direction on the sky. Moreover, for any given direction, there is a difference between attainable position, proper motion, and parallax accuracy: end-of-life position and proper motion errors will be, respectively, 21% and 44% smaller than end-of-life parallax errors.

2. The properties of Gaia's optical and detector system are such that for stars brighter than $V \sim 12$ mag, photon noise settles to a low level. The end-of-mission astrometric accuracies for these stars will amount to a few μas (the 'bright-star noise floor'). For magnitudes between $V \sim 12$ and 20 mag, photon noise determines the line-spread-function centroiding accuracies, and the expected end-of-life astrometric accuracies are $10-20$ μas at $V = 15$ and a few hundred μas at $V \sim 20$ mag (see the Appendix). At fainter magnitudes, star detection and confirmation statistics and sky-background effects enter, and astrometric accuracies reach milli-arcsecond (mas) levels.

3. At a given V magnitude, astrometric accuracy also depends on apparent star colour (i.e., intrinsic star colour combined with interstellar reddening) through, e.g., the wavelength-dependent properties of the CCD charge diffusion modulation transfer function (partly responsible for the 'image quality') and quantum efficiency of the CCDs and the transmission of the telescope optics. Generally, redder stars, at a given V magnitude, have smaller astrometric errors.

*On behalf of the Astrometry and Astrometric Error Budget Working Group

Key words: Gaia; Astrometry; Accuracy.

1. INTRODUCTION

Gaia's main goal is to collect high-precision astrometric data (i.e., positions, parallaxes, and proper motions) for the brightest $\sim$1 billion (10^9) objects in the sky. These data, complemented with multi-band, multi-epoch photometric and spectroscopic data collected from the same observing platform (see, e.g., Jordi 2004; Katz 2004) will allow astronomers to reconstruct the formation history, structure, and evolution of the Galaxy (see, e.g., Mignard 2004; Binney 2004). In the Gaia Concept and Technology Study Report (CTSR; ESA 2000), it was shown that meeting these main mission objectives will require the observation of a complete sample of stars down to $V \sim 20$ mag combined with end-of-life astrometric accuracies of 10 μas (or better) at $V = 15$ mag.

Order-of-magnitude estimates of Gaia's expected end-of-life astrometric accuracy are easily obtained by using 'back-of-the-envelope calculations' involving overall, system-level parameters such as primary mirror (pupil) size, detector efficiency, and mission lifetime (see, e.g., Lindegren 2002b). In the current system definition and detailed design phase of the project, however, a full-fledged astrometric accuracy tool is indispensable for carefully assessing the impact of various design alternatives on the scientific value of the mission product, for optimising instrument parameters such as the mirror coating reflectivity, and for safeguarding the mission objectives in general. It has been the responsibility of the Astrometry and Astrometric Error Budget Working Group to set up, maintain, and expand such a general astrometric accuracy model.

The astrometric accuracy model currently in place, known as the Gaia Astrometric Accuracy Tool (GAAT), provides a simplified yet realistic end-to-end simulation of the Gaia observation process, ranging from photon emission at the astronomical source at the one end, through the effects introduced by, e.g., the revolving scanning law and CCD time-delayed integration (TDI) operation, to single-transit centroiding measurements of the line spread function (LSF), and the averaging of these results over the operational mission lifetime at the other end (de Bruijne 2003a, 2003b, 2004b). The model also

includes, among others, wave-front errors (WFEs) due to optical aberrations and further image smearing due, among others, to transverse motion of sources in the focal plane and charge diffusion in the CCD detectors. Results derived with this tool give confidence that the present design of the satellite, referred to as the Gaia-2 design, is viable and that the scientific mission objectives can be met. The longer-term goal of the GAAT modelling effort is to include all effects affecting the final mission accuracies (see, e.g., Lindegren 2002a) and to expand the model to include photometric and radial velocity accuracy assessments as well.

This paper is aimed at describing the main properties of Gaia's astrometric accuracy, based on the latest GAAT results, tabulated in the Appendix. The GAAT software package itself is described in detail in de Bruijne (2003a, 2003b, 2004b). Section 2 of this paper introduces a simple formula — used as basis equation in GAAT — for establishing Gaia's end-of-mission accuracy. The importance of the scanning law is discussed in Section 3. Section 4 describes how astrometric accuracy for a given type of star depends on magnitude. The influence on astrometric accuracy of observed star colour — determined by spectral type plus interstellar reddening — is described in Section 5.

2. OVERVIEW AND BASICS

Consider a 'perfect' astronomical source, i.e., a single star, without companions and/or planets, that is photometrically non-variable, has a well-behaved spectrum, does not 'suffer' from micro-lensing, etc. For such an object, Gaia's end-of-mission astrometric accuracy σ, expressed in μas, can be calculated, to first order, as (see, e.g., Equation 66, p. 261, in ESA 2000):

$$\sigma = m \cdot g \cdot \sqrt{\frac{\tau}{N_{\rm tel} \cdot T \cdot p_{\rm det}(G)} \cdot \left(\sigma_\xi^2 + \sigma_{\rm cal}^2\right)}, \quad (1)$$

where

- m denotes an overall, end-of-mission contingency margin (Gaia-2 baseline assumption: $m = 1.2$, i.e., 20% margin);
- g is a dimensionless geometrical factor relating the scanning geometry to the determination of the astrometric parameters, discussed in detail in Section 3 (Gaia-2 baseline, averaged over the sky: $g = 1.51$ for positions, $g = 1.91$ for parallaxes, $g = 1.06$ for proper motions);
- $N_{\rm tel}$ is the number of astrometric instruments (viewing directions/telescopes; Gaia-2 baseline: $N_{\rm tel} = 2$);
- $T = (1 - L_{\rm dead}) \cdot L \cdot \Omega/4\pi$, expressed in units of s, is the (average) total observing time available per object and per instrument (Gaia-2 baseline: $T = 1513$ s);
- L, expressed in units of s, denotes the mission length, counted from the start of scientific observations at $t_0 = {\rm J2010.0}$. The quantity $L_{\rm dead}$ denotes the fraction of the mission length for which, for whatever reason, scientific data will not be available during the on-ground processing (see also Section 3; Gaia-2 baseline: $L = 5$ yr and $L_{\rm dead} = 0.10$, i.e., 10% dead time);
- Ω, expressed in units of steradians, denotes the effective solid angle of all astrometric field (AF) CCD detectors in the focal plane (excluding along-scan and across-scan dead zones between CCDs; Gaia-2 baseline: $\Omega = 0.44$ deg^2, using $N_{\rm strip} = 11$ CCDs, $N_{\rm row} = 10$ CCDs, 4500 lines per CCD, 1966 columns per CCD, 10×30 μm^2 pixels, Astro telescope focal length $F = 46.7$ m);
- τ, expressed in units of s, denotes the single-CCD transit time (Gaia-2 baseline: $\tau = 3.313$ s, using 4500 lines per CCD, scan rate $\omega = 60$ arcsec s^{-1}, Astro telescope focal length $F = 46.7$ m);
- $p_{\rm det}(G)$ is the ASM detection 'plus' AF1 confirmation probability as a function of the white-light Gaia G magnitude, in the current design only relevant (i.e., <1) for $G \gtrsim 20.3$ mag (see Arenou & Lim 2003);
- $\sigma_\xi^2 = \sigma_\xi^2(G)$, expressed in units of μas^2, denotes the variance of the LSF centroiding (localisation) process as a function of Gaia G magnitude for a single-CCD transit, discussed in detail in Sections 4 and 5; and
- $\sigma_{\rm cal}$, expressed in units of μas, is a constant ad-hoc calibration term, introduced in the absence (in GAAT) of a rigorous geometrical calibration model of the focal plane and calibration models for chromaticity correction, the on-ground satellite attitude reconstruction, thermo-mechanical stability of the telescope/instrument/focal plane, and basic angle variations (Gaia-2 baseline assumption: $\sigma_{\rm cal} = 40$ μas; see Section 7.4.3 in ESA 2000 for details).

The quantity $N_{\rm tel} \cdot T/\tau$ is the (average) total number of CCD crossings of an object during the mission, so that $N_{\rm eff} \equiv N_{\rm tel} \cdot T \cdot p_{\rm det}(G)/\tau$ is the expected (average) number of **detected** CCD crossings on which the estimation of its astrometric parameters is based. As a result, Equation (1) can also be written as:

$$\sigma = m \cdot g \cdot \sqrt{\frac{\sigma_\xi^2 + \sigma_{\rm cal}^2}{N_{\rm eff}}}. \quad (2)$$

The quantity $N_{\rm eff}$ should be interpreted as $N_{\rm eff} = N_{\rm strip} \cdot N_{\rm transit}$, where $N_{\rm strip}$ denotes the number of AF CCD strips in the focal plane and $N_{\rm transit}$ denotes the (average) end-of-mission total number of focal plane transits (for all $N_{\rm tel}$ instruments combined). As will be shown in Section 3, the current Gaia-2 baseline with $N_{\rm strip} = 11$ CCDs returns $N_{\rm eff} = 909$ CCD crossings (both instruments combined) and $N_{\rm transit} = 83$ focal plane transits (both instruments combined).

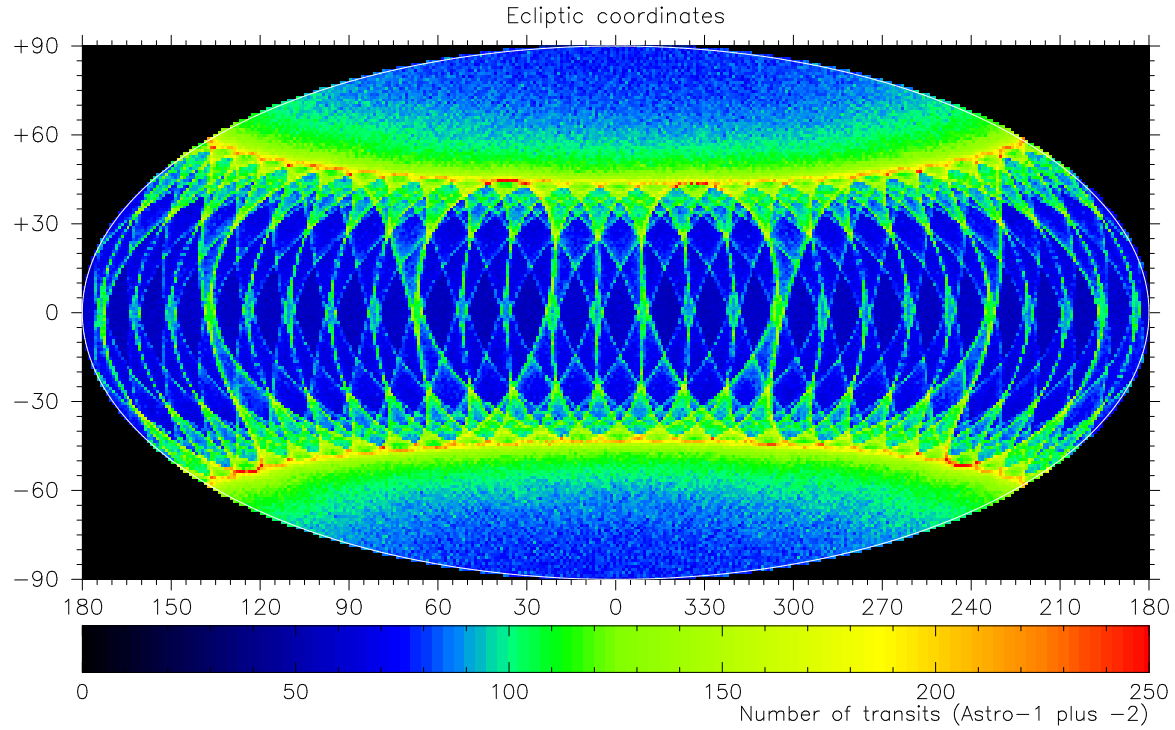

Figure 1. Dependence of the total end-of-mission number of focal plane transits ($N_{\rm transit}$) on position on the sky. Shown is an all-sky equal-area Hammer projection in ecliptic coordinates. The graduated colour coding corresponds to $N_{\rm transit}$, which refers to the total number of transits for the $N_{\rm tel}$ =2 telescopes combined (assuming $p_{\rm det}$ =1). The sky-average value of $N_{\rm transit}$ is 83 focal plane transits. The mission length is 5 year, 10% of which is assumed to be dead time.

3. INFLUENCE OF THE SCANNING LAW

Gaia's (nominal) scanning law is a central element in the data acquisition strategy during the $L = 5$-year operational lifetime of the satellite and the end-of-mission astrometric accuracies depend on its properties. Given technical boundary conditions — mainly related to the size of the sun shield and solar-panel power generation requirements — the scanning law has been defined in such a way that the precession speed of the spin axis on the sky is minimized and the uniformity of the end-of-mission sky coverage is maximized (see, e.g., Lindegren 1998a, 1998b, 2001). Nonetheless, the characteristics of this uniform revolving scanning law imply that astrometric accuracy varies with direction on the sky.

The factor g in Equations (1) and (2) relates the scanning geometry to the determination of the astrometric parameters. It is different for each of the five astrometric parameters (parallax [g_π], the position at the mean epoch of the mission in two coordinates [g_0, averaged over the two coordinates], and the proper motion components in two coordinates [g_μ, averaged over the two coordinates]) and varies as a function of position in the sky, mainly as a function of ecliptic latitude β (see, e.g., Figures 2–7 in Lindegren 1998b). Simulations of the scanning law have been used to determine the mean values (over the sky) of g_0, g_π, and g_μ for the current set of mission parameters, and their variations with ecliptic coordinates (see below). We assumed the current Gaia-2 baseline design: $\xi = 50^\circ$ = solar aspect angle, $\omega = 60$ arcsec s^{-1} = scan rate, $K = 5.2$ = number of spin-axis revolutions per Julian year around the solar direction (precession period = $365.25/K = 70.24$ days), and $S = 4.095$ = speed of the spin axis on the sky; the initial spin and revolving phases, corresponding to the start of scientific observations at $t_0 = {\rm J2010.0}$, were arbitrarily chosen as $\Omega(t_0) = \Omega_0 = 0$ and $\nu(t_0) = \nu_0 = 0$. The choice $S = 4.095$ has two important implications:

1. With this speed of the spin axis on the sky, each Julian year contains $K = 5.2$ revolutions ('loops') of the spin axis around the solar direction precisely. Since this value of K is not an integer, this spin-axis 'loop pattern' is not repetitive from year to year. The choice $S = 4.095$ thus avoids a scanning-law resonance/degeneracy (see Lindegren 1998a for details).

2. With $K = 5.2$, the product $K \cdot L = 5.2 \cdot 5 = 26$ is an integer. This means that, over the mission life, the spin axis makes exactly an integer number of revolutions around the solar direction, thereby optimising the uniformity of the end-of-mission sky coverage (see Lindegren 1998a for details).

With the assumption that 10% of the $L = 5$-year mission length will not contribute scientific observations to the on-ground data processing — due to, e.g., unplanned ground-station unavailability, spacecraft orbit maintenance, micro-meteorite impacts, payload inactivity during solar flares, contaminated windows due to prompt particle events (cosmic rays or solar protons), downlink

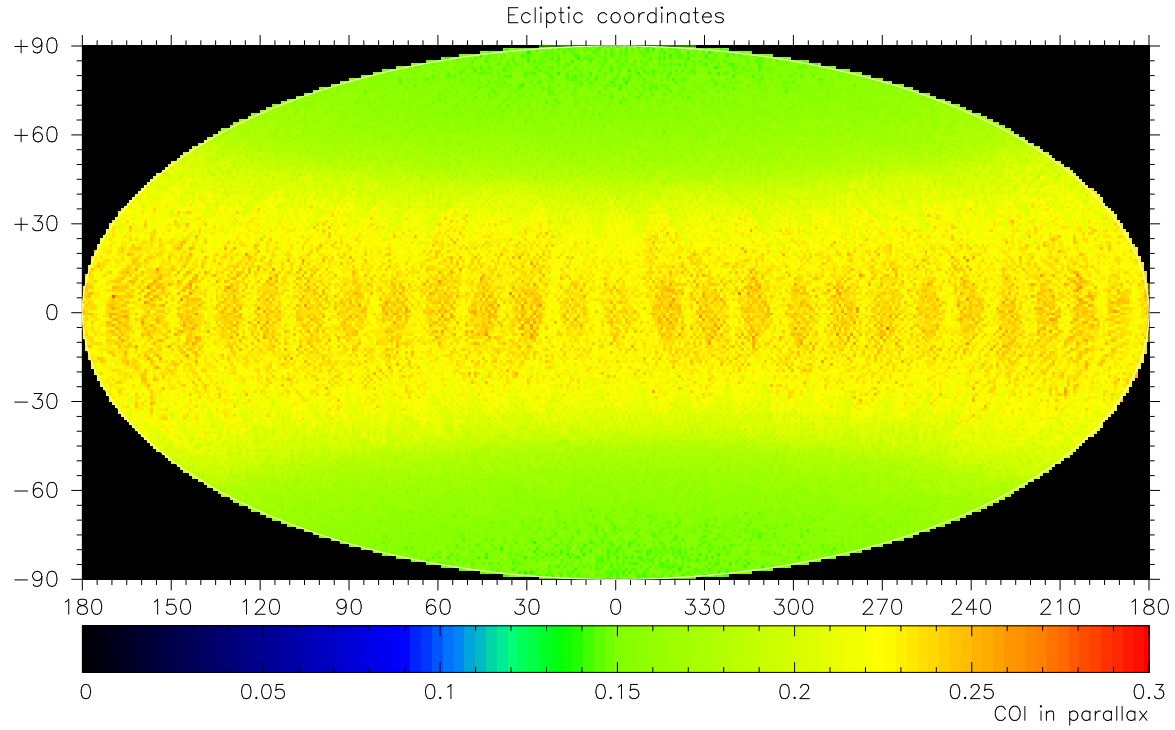

Figure 2. Dependence of the parallactic coefficient of improvement (COI) on position on the sky. Shown is an all-sky equal-area Hammer projection in ecliptic coordinates. The graduated colour coding corresponds to $\mathrm{COI}_\pi \equiv g_\pi/\sqrt{N_{\mathrm{transit}}}$ *(see also Figure 1), where* g_π *denotes the geometrical parallax factor. The sky-average value of* g_π *is 1.91 (for* ξ *=50°).*

telemetry losses, on-board data storage capacity limitations, etc — we find from the scanning-law simulations that the total end-of-mission number of focal plane transits, for both Astro telescopes together and without taking losses due to star detection probability into account (i.e., assuming $p_{\mathrm{det}}(G) = 1$), varies over the sky between 38 and 232, with a sky-average value of $N_{\mathrm{transit}} = 83$. The full dependence of N_{transit} on position in the sky is shown in Figure 1. With $N_{\mathrm{strip}} = 11$ AF CCD strips in the focal plane contributing to the astrometric accuracy budget, this gives $N_{\mathrm{eff}} = N_{\mathrm{strip}} \cdot N_{\mathrm{transit}} = 11 \cdot 83 = 909$ CCD transits (both instruments combined). With reference to Equation (2), we conclude that, to first order, the single-CCD-transit centroiding error σ_ξ is reduced, at the end of the mission, by a factor $\sqrt{N_{\mathrm{eff}}} = \sqrt{909} = 30$.

Scanning-law simulations yield the following sky-averaged geometrical factors and, in brackets, their variations over the sky:

- $g_0 = 1.51$ (g_0 varies over the range 1.42–1.99),
- $g_\pi = 1.91$ (g_π varies over the range 1.30–3.10),
- $g_\mu = 1.06$ (g_μ varies over the range 0.82–1.67).

Figure 2 shows, as an example, how $g_\pi/\sqrt{N_{\mathrm{eff}}}$ — known as the parallactic coefficient of improvement (COI; see, e.g., Lindegren 1998b) — varies over the sky in ecliptic coordinates. The observed pattern is entirely due to the scanning law. The geometrical parallax factor g_π depends on the solar aspect angle ξ (baseline: $50°$) as $g_\pi \sim 1.47/\sin\xi$ for $45° \leq \xi \leq 60°$ (see also de Bruijne 2004a and Equation 67 in ESA 2000).

Since $g_\mu < g_0 < g_\pi$, there is a significant difference between attainable position, proper motion, and parallax accuracy for any given direction. We find g_0/g_π $(= \sigma_0/\sigma_\pi) = 0.79$ and g_μ/g_π $(= \sigma_\mu/\sigma_\pi) = 0.56$. Thus, end-of-life (random) position and proper motion errors are, respectively, 21% and 44% smaller than end-of-life (random) parallax errors.

With our findings, and setting $p_{\mathrm{det}}(G) = 1$, Equation (2), applied to the current Gaia-2 baseline design, can be simplified to:

$$\begin{aligned} \sigma_\pi\ [\mu\mathrm{as}] &= m \cdot g_\pi \cdot \sqrt{\frac{\sigma_\xi^2 + \sigma_{\mathrm{cal}}^2}{N_{\mathrm{eff}}}} \\ &= 1.2 \cdot 1.91 \cdot \sqrt{\frac{\sigma_\xi^2 + 40^2}{909}} \\ &= 0.076 \cdot \sqrt{\sigma_\xi^2 + 40^2}, \end{aligned} \qquad (3)$$

where $\sigma_\xi = \sigma_\xi(G)$ denotes the single-CCD-transit centroiding error for a star with magnitude G. This quantity, and notably its dependence on magnitude, is discussed in Sections 4 and 5.

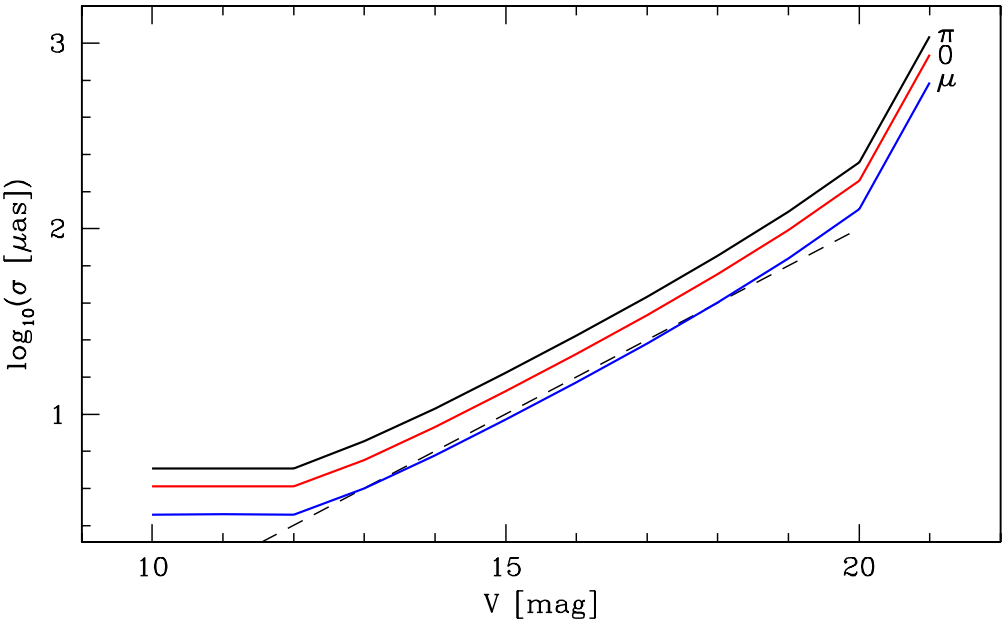

Figure 3. End-of-mission astrometric accuracy predictions, for the current Gaia-2 baseline design, as a function of V magnitude for an unreddened solar-type star (spectral type G2V). The dashed line refers to the top-level mission requirement, i.e., $\sigma = 10$ μas at $V = 15$ mag, extrapolated to other magnitudes assuming centroiding accuracies are photon-noise limited.

4. INFLUENCE OF MAGNITUDE

4.1. Bright Stars

The properties of Gaia's optical and detector system (see, e.g., Short 2004) are such that for stars brighter than $V \sim 12$ mag, saturation at CCD level sets in. (Since the CCDs operate in the Gaia G-band, and not in the Johnson V-band, saturation actually sets in at $G \sim 12$ mag; this distinction is ignored in Section 4 and discussed in Section 5.) Saturation is currently foreseen to be handled by activating TDI gates for bright stars. A TDI gate is a specific CCD line where the 'continuous' TDI-driven along-scan charge transfer can be temporarily 'held and reset'. At read out, bright-star samples thus only contain charges collected during a fraction of the full CCD transit time of 3.313 s (4500 lines). The Astro CCDs currently contain 12 strategically positioned TDI gates, increasing the bright-star limiting magnitude from $V \sim 12$ mag to $V \sim 4$ – 6 mag. In the bright-star regime, $N_{\rm electron}$, defined as the total number of electrons in the point spread function (PSF) at CCD read out, thus does not increase for increasingly brighter stars.

The photon noise for bright stars has only a modest effect on the centroiding errors σ_ξ, which can reach millipixel levels (the current design has $\sigma_{\xi,\rm min} \sim 60$ μas), and calibration errors, quantified by $\sigma_{\rm cal} = 40$ μas, become apparent. With $\sigma_\xi = 0$ μas, Equation (3) returns:

$$\sigma_{\pi,\rm cal}\ [\mu{\rm as}] = 0.076 \cdot 40 = 3.0\ \mu{\rm as},$$

which can be considered as the end-of-life 'calibration parallax noise floor'. Including a minimum centroiding error $\sigma_{\xi,\rm min} = 60$ μas in Equation (3) returns the end-of-mission 'bright-star noise floor':

$$\sigma_{\pi,\rm min}\ [\mu{\rm as}] = 0.076 \cdot \sqrt{60^2 + 40^2} = 5.5\ \mu{\rm as}.$$

Astrometric accuracies for bright stars thus amount to a few μas (see the Appendix).

4.2. Faint Stars

For magnitudes between $V \sim 12$ and 20 mag, photon noise effectively determines the LSF centroiding accuracies σ_ξ. For the faintest stars, it is currently foreseen to transmit, for each CCD, the 'central' six along-scan samples to the ground (see, e.g., Høg 2004). Dedicated Monte Carlo simulations using a custom-developed maximum likelihood centroiding algorithm (see, e.g., Lindegren 2000) indicate that the formal Cramér–Rao bound — corresponding to the theoretical limit on the centroiding precision — can be reached with 6-sample windows in Gaia's current design.

Since, ideally, $\sigma_\xi \propto N_{\rm electron}^{-1/2}$ and $V \propto G \propto -2.5 \cdot \log_{10} N_{\rm electron}$ for a given star (see also Section 5), we expect $\log_{10}\sigma \propto V$, where the proportionality constant equals $-\frac{1}{2}/-2.5 = 0.2$. The expected end-of-life parallax accuracies σ_π are 10 – 20 μas at $V = 15$ mag and (thus) a few hundred μas at $V = 20$ mag (see the Appendix).

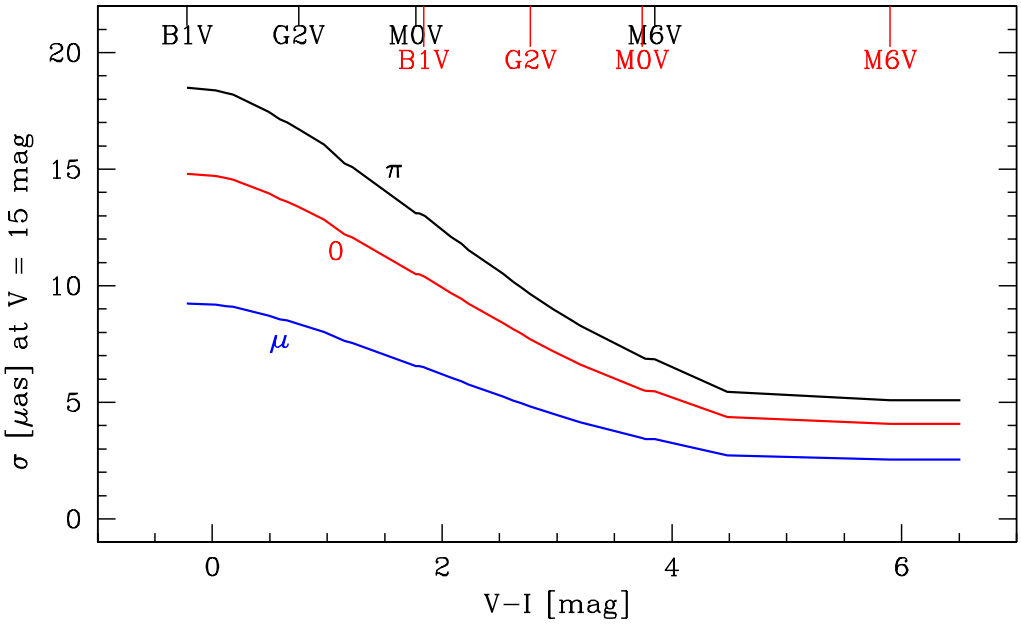

Figure 4. Dependence of end-of-mission astrometric accuracy σ on apparent $V-I$ star colour at $V = 15$ mag. The three lines refer to position, parallax, and proper motion accuracies. The vertical ticks on the top axis, and the labels, indicate $V-I$ colours for B1V, G2V, M0V, and M6V stars. The upper labels and short ticks refer to unreddened stars, while the lower labels and long ticks refer to reddened stars with $A(550\ \mathrm{nm}) = 5$ mag.

4.3. Faintest Stars

For stars fainter than $V \sim$20 mag, two additional effects degrade astrometric accuracy further. These are (1) the sky background (and CCD total detection noise), and (2) the finite star detection and confirmation statistics.

1. At $V = 20$ mag, an unreddened A0V star, for example, contains a total number of $N_{\mathrm{electron}} = 171$ electrons in the PSF, compared to 232 sky-background photo-electrons in the 6-sample window allocated to that star. The increased relative importance of the sky background for fainter stars, and the associated increase in the total photonic (Poisson) noise, decreases the centroiding precision σ_ξ and thus the end-of-mission astrometric accuracy. Similar arguments hold for the CCD total detection noise (comprising readout noise, video chain noise, dark noise, etc), currently expected to be 5 – 7 e^-, which gains in relative importance for fainter stars.

2. At $V = 20$ mag, an unreddened A0V star, for example, has a detection and confirmation probability of 100%. At $V = 21$ mag, however, this probability has reduced, due to the special sampling and associated limited signal-to-noise with which the ASM detection and AF1 confirmation CCDs operate, to a meager 6%. (Since the detection and confirmation CCDs operate — like all Astro AF CCDs — in the reddish Gaia G-band, and not in the Johnson V-band, detection and confirmation probabilities are higher, for a given V magnitude, for apparently redder stars; see Section 5 for details.) This reduced probability translates directly into a reduced number of focal plane transits and thus degrades end-of-mission astrometric accuracy (see Equation 1).

The combined action of the above-mentioned effects can cause astrometric accuracies to reach milli-arcsecond levels at the faintest magnitudes ($V \gtrsim 20$ mag; see the Appendix).

4.4. Summary

Figure 3 shows the predicted end-of-mission astrometric accuracies σ for positions, parallaxes, and proper motions as a function of V magnitude. The three solid curves refer to the current Gaia-2 baseline design and are valid for an unreddened solar-type star (spectral type G2V). The dashed line in Figure 3 refers to the top-level mission requirement on astrometric accuracy, i.e., $\sigma \leq 10$ μas at $V = 15$ mag. The behaviour of the solid curves clearly reflects the three magnitude regimes described in Sections 4.1–4.3:

4.1 The bright-star regime (4–6 $\lesssim V \lesssim$ 12 mag) where performance is set by bright-star centroiding and calibration errors;

4.2 The faint-star, photon-noise regime (12 $\lesssim V \lesssim$ 20 mag) where the centroiding error, and thus the end-of-mission accuracy, scales as $\sigma = 10^{0.2 \cdot V}$; and

4.3 The faintest-star regime ($V \gtrsim 20$ mag) where finite star detection and confirmation probabilities, sky background, and total detection noise degrade astrometric accuracy further.

5. INFLUENCE OF OBSERVED STAR COLOUR

It has been demonstrated in Section 4 that the LSF centroiding precision σ_ξ is inversely proportional to the square root of the total number of photo-electrons in the LSF:

$$\sigma_\xi \propto N_{\rm electron}^{-1/2}$$

By definition, and independent of star type and colour, the base-10 logarithm of $N_{\rm electron}$ is directly proportional to the white-light, broad-band Gaia G magnitude (itself defined by the transmission of the Astro telescope optics and the detector response, i.e., the CCD quantum efficiency):

$$G \propto -2.5 \cdot \log_{10} N_{\rm electron}$$

It thus follows that the centroiding precision σ_ξ, when considering a variety of stars with various apparent colours, is a unique function of Gaia G magnitude (but not of Johnson V magnitude, or any other magnitude). Inverting this line of reasoning, it follows that, at a given V magnitude (e.g., $V = 15$ mag), astrometric accuracy depends on apparent star colour, i.e., on intrinsic star colour (spectral type) and on interstellar reddening. Figure 4 confirms this 'claim'.

Figure 4 shows how σ for a star with $V = 15$ mag depends on its observed $V - I$ colour. The three lines refer to the end-of-mission astrometric accuracies for positions, parallaxes, and proper motions. The vertical 'displacements' of the three curves reflect our earlier finding that $g_\mu < g_0 < g_\pi$ (see Section 3). The flattening off of the curves at low values of σ towards higher values of $V - I$ reflects the fact that progressively redder stars, at $V = 15$ mag, start to reach the noise floor at $G \sim 12$ mag (see Section 4.1). The following example demonstrates this (see also the Appendix):

- An unreddened early-type B1V star has $V - I = -0.22$ mag and $V - G = -0.01$ mag, i.e., $V = 15$ mag corresponds to $G = 15.01$ mag;
- An unreddened late-type M6V star has $V - I = 3.85$ mag and $V - G = 2.39$ mag, i.e., $V = 15$ mag corresponds to $G = 12.61$ mag.

At the same V magnitude, the red star thus appears relatively 'bright' to Gaia compared to the blue star and its end-of-mission astrometric accuracy is thus higher (the error σ is smaller). The top axis of Figure 4 displays vertical tick marks for (two sets of) four different stars: B1V, G2V, M0V, and M6V. The upper labels refer to unreddened stars, while the lower labels refer to reddened stars (we assumed $A(550\ {\rm nm}) = 5$ mag). Figure 4 confirms that redder stars have smaller astrometric errors at a fixed V magnitude, basically reflecting the fact that Gaia's photometric G band, in which the astrometric observations are made, is a red and not a visible band.

ACKNOWLEDGMENTS

It is a pleasure to thank the Scientific and Local Organising Committees, chaired by Catherine Turon, Michael Perryman and Yves Viala, for orchestrating an enjoyable symposium. Lennart Lindegren and Michael Perryman are gratefully acknowledged for their stimulating support and their guidance and inputs received during the development of the Gaia Astrometric Accuracy Tool.

REFERENCES

Arenou, F., Lim, J.–C., 2003, Gaia technical report OBD-FAJCL-001

Binney, J., 2005, ESA SP-576, this volume

de Bruijne, J.H.J., 2003a, Gaia technical report Gaia-JdB-006

de Bruijne, J.H.J., 2003b, Gaia technical report Gaia-JdB-008

de Bruijne, J.H.J., 2004a, Gaia technical report Gaia-JdB-012

de Bruijne, J.H.J., 2004b, Gaia technical report Gaia-JdB-016

ESA, 2000, 'Gaia Concept and Technology Study Report' (CTSR), ESA–SCI(2000)4

Høg, E., 2005, ESA SP-576, this volume

Jordi, C., 2005, ESA SP-576, this volume

Katz, D., 2005, ESA SP-576, this volume

Lindegren, L., 1998a, Gaia technical report Gaia-LL-014 (erratum Gaia-LL-014A)

Lindegren, L., 1998b, Gaia technical report Gaia-LL-026

Lindegren, L., 2000, Gaia technical report Gaia-LL-032

Lindegren, L., 2001, Gaia technical report Gaia-LL-035

Lindegren, L., 2002a, Gaia technical report Gaia-LL-040

Lindegren, L., 2002b, Gaia technical report Gaia-LL-043, version 1

Mignard, F., 2005, ESA SP-576, this volume

Short, A., 2005, ESA SP-576, this volume

APPENDIX: GAIA PERFORMANCE PREDICTIONS (GAIA-2 DESIGN, NOVEMBER 2004)

The table below summarises predicted Gaia-2 end-of-mission parallax accuracies σ_π, expressed in units of μas, as a function of V magnitude. The top half of the table refers to unreddened stars; the bottom half of the table refers to reddened stars. Accuracies have been calculated using the Gaia Astrometric Accuracy Tool (GAAT) for the current Gaia-2 baseline design (November 2004). The data include a 20% overall contingency ($m = 1.2$) and assume a 10% dead time ($L_{\rm dead} = 0.10$). Other assumptions and mission/payload parameters are summarised in Sections 2–3.

Spec. type	$V-G$	$V-I$	$V=$ 10	11	12	13	14	15	16	17	18	19	20	21
$A(550\ \mathrm{nm}) = 0$ mag														
B1V	−0.01	−0.22	5.4	5.4	5.9	8.6	13.2	20.7	34.1	54.9	90.6	156.3	290.0	2812.4
A0V	0.01	0.03	5.4	5.4	5.9	8.6	13.2	20.6	32.8	54.6	90.1	155.5	287.7	2474.0
A3V	0.03	0.12	5.4	5.4	5.9	8.5	13.1	20.5	32.5	54.2	89.4	154.2	285.3	2190.4
A5V	0.04	0.18	5.4	5.4	5.9	8.5	13.0	20.4	32.4	54.0	89.1	153.5	283.4	2070.1
F2V	0.13	0.49	5.4	5.4	5.7	8.2	12.5	19.6	31.1	51.6	85.0	145.8	268.1	1478.4
F6V	0.17	0.59	5.4	5.4	5.6	8.1	12.3	19.3	30.6	50.7	83.3	142.7	260.9	1367.7
F8V	0.19	0.65	5.4	5.4	5.6	8.0	12.2	19.1	30.3	50.2	82.4	141.1	257.7	1309.5
G2V	0.23	0.75	5.4	5.4	5.6	7.9	12.0	18.7	29.8	49.3	80.8	138.1	251.4	1195.7
K3V	0.44	1.15	5.4	5.4	5.4	7.3	11.0	17.2	27.1	44.8	73.0	123.5	222.0	707.3
M0V	0.79	1.77	5.4	5.4	5.4	6.5	9.6	14.8	23.3	38.2	61.8	103.2	181.2	345.5
M6V	2.39	3.85	5.4	5.4	5.4	5.4	5.5	7.8	11.7	18.2	28.9	47.5	77.8	132.5
G8III	0.33	0.97	5.4	5.4	5.5	7.7	11.6	18.0	28.6	47.1	77.2	131.2	237.3	1049.4
K3III	0.46	1.22	5.4	5.4	5.4	7.3	10.9	17.0	26.9	44.3	72.3	122.2	219.2	631.8
M0III	0.79	1.80	5.4	5.4	5.4	6.5	9.6	14.8	23.3	38.2	61.8	103.1	181.2	343.5
M7III	3.04	4.48	5.4	5.4	5.4	5.4	5.4	6.1	9.0	13.7	21.5	34.3	56.8	94.1
B0I	−0.01	−0.21	5.4	5.4	5.9	8.6	13.2	20.7	34.1	55.0	90.8	156.6	290.3	2808.1
$A(550\ \mathrm{nm}) = 5$ mag														
B1V	0.80	1.84	5.4	5.4	5.4	6.5	9.6	14.8	23.2	38.0	61.6	102.8	180.3	342.7
A0V	0.98	2.08	5.4	5.4	5.4	6.1	8.9	13.7	21.6	35.2	56.8	94.1	163.5	306.1
A3V	1.04	2.17	5.4	5.4	5.4	6.0	8.7	13.4	21.0	33.4	55.2	91.3	158.1	295.0
A5V	1.09	2.23	5.4	5.4	5.4	5.9	8.6	13.1	20.5	32.7	53.9	89.0	153.9	285.3
F2V	1.31	2.53	5.4	5.4	5.4	5.5	7.9	11.9	18.6	29.5	48.5	79.6	135.8	247.9
F6V	1.39	2.62	5.4	5.4	5.4	5.5	7.7	11.5	18.0	28.5	46.8	76.6	130.3	236.7
F8V	1.44	2.68	5.4	5.4	5.4	5.4	7.5	11.3	17.6	27.9	45.8	74.8	127.0	229.6
G2V	1.52	2.77	5.4	5.4	5.4	5.4	7.3	11.0	17.0	26.9	44.1	72.0	121.8	218.9
K3V	1.82	3.13	5.4	5.4	5.4	5.4	6.5	9.7	14.9	23.4	38.2	62.0	103.6	182.0
M0V	2.36	3.74	5.4	5.4	5.4	5.4	5.5	7.9	11.9	18.5	29.3	48.1	79.0	135.0
M6V	4.50	5.90	5.5	5.5	5.5	5.5	5.5	5.5	5.5	7.6	11.4	17.7	28.1	46.2
G8III	1.69	2.97	5.4	5.4	5.4	5.4	6.9	10.2	15.8	24.9	40.7	66.2	111.1	197.2
K3III	1.89	3.20	5.4	5.4	5.4	5.4	6.4	9.4	14.5	22.7	37.1	60.0	100.0	175.0
M0III	2.38	3.77	5.4	5.4	5.4	5.4	5.5	7.8	11.7	18.2	29.0	47.6	78.0	132.8
M7III	5.21	6.51	5.5	5.5	5.5	5.5	5.5	5.5	5.5	5.9	8.6	13.0	20.4	32.4
B0I	0.81	1.85	5.4	5.4	5.4	6.5	9.6	14.7	23.2	37.9	61.4	102.4	179.7	341.0